

# Position Estimation and Control of Compact BLDC Motors Based on Analog Linear Hall Effect Sensors

Alex Simpkins<sup>†</sup> and Emanuel Todorov<sup>‡</sup>

**Abstract**—Bio-mimetic robotic systems, among many other engineered systems, require motors which possess high torque, little or no torque ripple, compact size, and precise position control. It is frequently challenging to include a motor with a design which fits all of these requirements. Several companies have recently released compact pancake brushless DC motors which possess excellent characteristics. However, ripple-free precision control of brushless motors requires precision position measurement. It can be difficult to mount encoders directly to the shafts of these motors, and for precision position control, a sensorless configuration may be inappropriate. We propose a novel method of measuring rotor position using analog Hall effect sensors to measure the magnetic field of the rotor magnets to create an absolute position measurement of the electrical cycle, which can be used efficiently to create a computationally simple motor control scheme. These Hall effect sensors are mounted directly to the motor and are highly compact, have high bandwidth, are extremely low cost, and have high precision, providing position measurements with insignificant increases to motor size.

## I. INTRODUCTION

Recently brushless DC (BLDC) motors[14] have gained tremendous popularity. They have been constructed in all shapes and sizes from very small - only a centimeter or less, to very large - motors requiring kiloWatts to run. BLDC motors are found in computer peripherals, surgical devices, portable pumps, robotics[12], haptics[5], and electric cars to name a few examples. As a result, many embedded systems manufacturers are providing application notes, technical papers, hardware to aid in development, and firmware designed to encourage engineers and scientists to use their products with the many BLDC motor applications.

One strength of these new BLDC motors is that they have high torque and can be purchased in a very compact size (for example, the Maxon EC series and Portescap NuvoDisk series). As a result they have been included in many robotics and compact industrial designs such as in [8] and [13] or most hard drives, optical drives, cooling fans, and more. For systems where the motor is to spin at a constant velocity and/or direction, there are many simple 'sensorless' control schemes[15] which can be used to drive the motor.

At high speeds torque ripple plays an insignificant role as well, and so for the constant speed/sensorless applications, there is less emphasis on unique position measurement and torque ripple compensation. But for applications where precision position control is important, and the system is highly compact - with minimal space surrounding the motor, it may be very difficult to mount standard sensors (encoders, potentiometers, etc). In addition, if one were to use standard sensors, the sensor commutation pattern must be repeated several times (electrical revolutions) per mechanical revolution. The number of repetitions varies per motor, and any position measurement must be mapped into

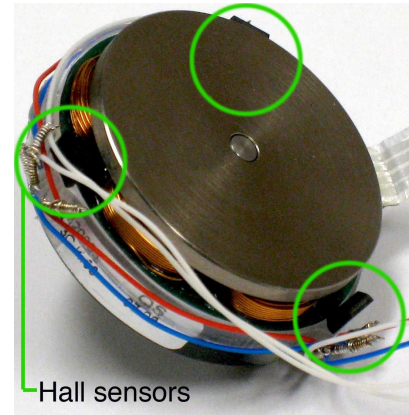


Fig. 1. A brushless DC pancake motor with linear Hall effect sensors arranged to provide precision rotor position information by measuring the rotor magnetic field.

the appropriate electrical revolution space. This requires microprocessor computation time. Advanced robotic systems require high performance controls to be running in realtime, coordinating communication, data acquisition, and control strategies. Where computation time can be saved, it should be.

For many applications which do not require precise position control, but when speed and direction vary, low resolution digital Hall effect sensors that output a binary signal are typically embedded within industrial motors. This is useful for simple commutation schemes such as block commutation. However, if the analog Hall sensor signal were outputted instead of the binary signal after careful design of the location and orientation of the Hall sensors, the motors would still be simple to produce (in fact, the entire closed loop servo system would be far simpler and less expensive), and better position control would be possible using the scheme proposed here. Therefore this practical method can have a potentially large real-world impact.

We present in this paper a novel methodology for detecting absolute (in electrical revolution coordinates) position of a BLDC motor using inexpensive analog Hall sensors, and a low computation time algorithm to extract position information. Further, this algorithm can be implemented in tandem with simple block commutation, sinusoidal commutation, or field oriented control. Finally, in cases where parameters in the system may vary due to imprecise mounting of the sensors, temperature variation, etc, an Extended Kalman Filter (EKF) based adaptive scheme is proposed and validated<sup>1</sup>.

The remainder of this paper is organized as follows. Section II presents the method of analog Hall sensor-based position measurement. Section III presents methods for effi-

<sup>1</sup>It is important to note that this method of measuring Hall sensors and determining position is quite effective without the adaptive scheme. The adaptive scheme is an additional technique to make this general method effective with noisy or biased measurements.

This work was supported by the US National Science Foundation  
<sup>†</sup>Department of Computer Science and Engineering, University of Washington, AC101 Paul G. Allen Center, Box 352350, 185 Stevens Way, Seattle, WA, 98195-2350, email: csimpkin@cs.washington.edu  
<sup>‡</sup>Department of Computer Science and Engineering, University of Washington, AC101 Paul G. Allen Center, Box 352350, 185 Stevens Way, Seattle, WA, 98195-2350, email: todorov@cs.washington.edu

ciently combining the position estimation method with block commutation, with sinusoidal commutation, and with sinusoidal commutation in tandem with an adaptive algorithm using an EKF. Section IV presents results comparing the implementations of the methods from Section III with the methods of Section II, then discusses the implications of these results. Finally, Section V concludes the paper with some remarks and future works.

## II. ANALOG HALL EFFECT SENSOR-BASED POSITION MEASUREMENT

### A. Review of the design of BLDC Motors

A BLDC motor has several advantages over the DC brushed motor design. These include higher torque, limited components to wear, no arcing, among others. The main components of a typical BLDC motor are displayed in Fig. 2. Essentially the BLDC motor is similar to the idea of an 'inside out' DC brushed motor. The magnets are housed in the rotor, and the stator houses the coils. Commutation must be performed electronically by sensing rotor angle relative to the coils and energizing appropriate coils to create an electromagnetic field which creates a resultant torque on the rotor.

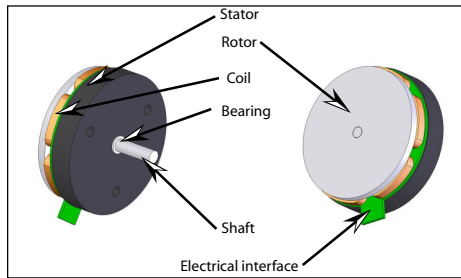


Fig. 2. A typical pancake BLDC motor. The magnets embedded within the rotor are suspended above the coils in the axial rather than radial direction.

### B. Introduction to Hall effect sensor-based position measurements

The main components of the method consist of mounting the sensors in a regular pattern around the motor (Fig. 1 and 3). One sensor is required per coil. The question arises as to why one can mount a sensor which measures magnetic field strength so close to the electromagnetic field (EMF) generated by the motor coils. There are two potential answers. The first is simply that the sensor measures field strength in a linear axis nearly orthogonal to the coil field. This can be verified theoretically and experimentally (see Section IV). The other implication of this is that the orientation of the Hall effect sensors relative to the coils and rotor magnets must be carefully determined in order to avoid interference from the time-varying magnetic field generated in the coils. The second answer is that the reluctance of the air is far higher than the reluctance of the motor components, so most of the flux field density (the magnetic circuit) due to coil currents remains within the motor. By measuring the analog Hall sensor signal directly, a high resolution rotor position can be extracted from that data. The notion of extracting an angular position from sinusoidal waveforms in general is not new. The concept is that of an older technology - the resolver. However, the present application differs in that the sensor and actuator are integrated (since the sinusoids are generated by the magnets embedded within the rotor, and the Hall sensors are attached to or integrated into the motor), and the measurement repeats with every electrical cycle,

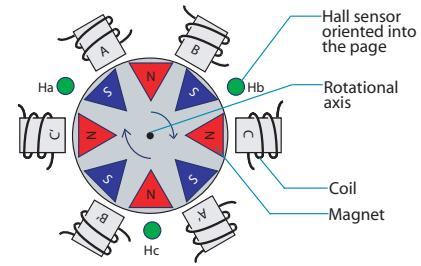


Fig. 3. A simplified representation of a brushless DC motor with three phases and four pole pairs. The magnets and coils are arranged in a radial direction.

not every mechanical cycle. For commutation purposes, it is central to have an absolute measure of where the rotor presently is at any sample time within the electrical cycle. This allows sinusoidal or any other form of commutation desired, as well as provides a position measurement of the robot joint associated with that particular motor.

### C. Relative angle estimation by quadrant determination

Assume an example BLDC motor (such as depicted in Fig. 1, and schematically in Fig. 3) which is constructed with three phases and four pole-pairs (4 sets of N-S magnets embedded in the rotor). This is key for determining the ratio of electrical cycles to mechanical revolutions. Considering one Hall sensor which outputs a voltage proportional to magnetic flux field density at a particular orientation and position, it is clear that one pole-pair (one north pole magnet at one rotor angle, and a south pole magnet positioned  $\pi$  radians apart along the outer radius of the rotor) will result in the measurement of a single sinusoid which repeats after one mechanical revolution. To commutate the coils, one would need to repeat a particular coil current pattern only once, and so there would be one electrical cycle per mechanical revolution.

The number of electrical cycles correspond to the number of pole-pairs of the rotor. Since we have four pole-pairs in this motor, there are four electrical cycles per mechanical revolution. This means that, since we have three Hall sensors mounted, we can uniquely determine position of the rotor (see Fig. 4(b)) within a  $\pi/2$  radian segment (one quarter of a revolution). In order to obtain a relative measure of angle which can exceed the  $\pi/2$  radian limit, one must build a software jump detector, which detects when a massive change in measured angle occurs (during a crossing of the boundary from one mechanical quadrant to another). An integer sine and arcsine lookup table are stored in memory (integer computations are used for speed, but one could also use floating point computations if a fast floating point DSP is available) and used along with trigonometric relationships to determine the rotor angle. At this point the values to be injected back into the coils for commutation can be phase shifted appropriately (Fig. 4(a)).

A more complex hardware setup could theoretically be used with a fixed phase advance by doubling the number of Hall sensors and offsetting them by the phase advance - one set for each intended direction of movement. Then the measurement of the Hall sensor could be directly injected back into the coils to produce continuous rotation in one or the other direction. Speed would be controlled simply by scaling the measurement before injecting it back into the coils.

Angle, phase, and Hall sensor measures are related in the following way (where  $n$  is the number of pole-pairs in the

BLDC motor's rotor,  $\phi$  is the phase of the three sensors,  $\psi_i$  is the individual phase for the specified sensor relative to the first,  $\theta$  is the position of the rotor (in mechanical revolution coordinates),  $\alpha$  and  $\beta$  are the minimum and maximum raw Hall sensor measures,  $v(t)$  is Gaussian noise with mean 0 and covariance  $\Omega_v$ , and  $r$  is the  $[-1, 1]$  normalized Hall measurement for a given sensor  $i$ ):

$$r_i(t) = \sin(n(\theta - \phi - \psi_i)) + v(t). \quad (1)$$

The raw measurement is related to the normalized measure as follows:

$$r_i(t) = 2 \frac{\bar{r}_i(t) - \alpha_i}{\beta_i - \alpha_i} - 1. \quad (2)$$

Thus, the raw sensor measurements can be related to angle directly, assuming the various sensor placements are known and static by combining the above two equations:

$$\bar{r}_i(t) = \frac{1}{2}(\beta_i - \alpha_i) \left( \sin(n(\theta - \phi - \psi_i)) + v(t) + 1 \right) + \alpha_i. \quad (3)$$

The angle, theta, can be computed from the raw sensor measurements (an absolute measure within  $\pi/2$  Rad), and the transitions between  $\pi/2$  increments kept track of to form a relative measure as follows (let us define  $\tilde{\theta}$  as the indirect observation of position based on Hall sensor signals, and note that  $\lfloor \cdot \rfloor$  represents the floor() function. Note we are using normalized hall measures for simplicity here, and that  $q$  represents the number of  $\pi/2$  quadrants crossed since the last reset of zero for  $\tilde{\theta}$ , and  $\dot{\theta}$  is the current angular velocity estimate)<sup>2</sup>:

$$\begin{aligned} \tilde{\theta}(t) &= \left[ q\pi/2 + \frac{1}{3n} \left( [\text{asin}(r_0) + \phi], \right. \right. \\ &\quad \left. \left. + [\text{asin}(r_1) + \phi + \psi_1], \right. \right. \\ &\quad \left. \left. + [\text{asin}(r_2) + \phi + \psi_2] \right) \right], \quad (4) \\ q(t) &= q + \text{floor} \left( \frac{1.8|\dot{\theta}|}{\pi} \right) \text{sign}(\dot{\theta}). \end{aligned}$$

The  $\tilde{\theta}$  equation can be considered to be an average between sensor measures. A simpler (computationally) implementation is

$$\tilde{\theta}(t) = q\pi/2 + \frac{1}{n} [\text{asin}(r_0) + \hat{\phi}], \quad (5)$$

which can then be averaged over several samples. If a perfect measure of  $\theta$  were available (this is the angle within a  $\pi/2$  quadrant we are interested in for the following), and there were no noise in the Hall sensor measurements, the relative sensor placements could be computed by

$$\begin{aligned} \theta &= \frac{1}{n} \text{asin}[r_0] + \phi, \quad (6) \\ \psi_1 &= -\frac{1}{n} \text{asin}[r_1] - \phi + \theta, \\ \psi_2 &= -\frac{1}{n} \text{asin}[r_2] - \phi + \theta. \end{aligned}$$

Though we need to estimate the measure of the previous three variables, the above relationships are useful in computing the estimates.  $\theta$  and  $\tilde{\theta}$  can be directly used with any commutation scheme given the parameters  $\phi$  and  $\psi_i$ . These parameters can be guessed or determined once, then held constant.

<sup>2</sup>Note that here we have dropped the noise term, as we are dealing with estimates, deterministic relations are used. The stochastic nature of the sensor measurements will be dealt with directly during the development of the EKF in Section III-C.

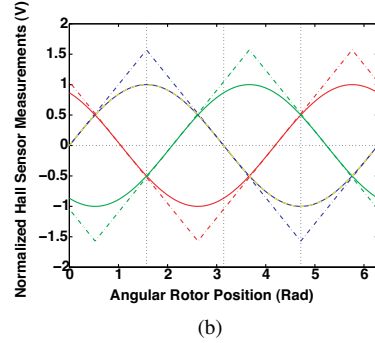
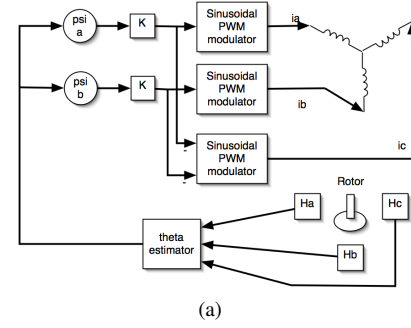


Fig. 4. (a) Motor controller basic block diagram for open loop current control. (b) Hall effect sensor signals (solid) showing the phase difference between coil ( $\pi/3$ ) A, B, and C, and the arcsine of each signal showing the periodic nature of the direct angular estimate. This emphasizes the need to recover the sector (using multiple sensors makes this possible) within the  $\pi/2$  radian quadrant where absolute position within that quadrant is known.

#### D. Effective resolution

The effective resolution (R) of the rotor angle estimate and number of counts per revolution (CPR) are found by computing the maximum peak-peak voltage ( $V_{pp}$ ) of the Hall effect sensors (which could be amplified to be at the maximum range of the analog to digital converter (ADC), then the ADC resolution (given  $V_{ss}$ - $V_{dd}$  voltage scaling), then dividing the  $V_{pp}$  by the resolution (below calcs given at 10 bit resolution, 12 bits are possible using the dsPIC implementation in this system[6], but that affects its ability to sample simultaneously):

$$\begin{aligned} V_{pp} &= 0.400V \quad (7) \\ V_{adc-res} &= 3.3V/1024 \\ CPR &= V_{pp}/V_{adc-res} * 4 \\ &= 1984 \\ R &= 360/1984 = 0.18^\circ \end{aligned}$$

12 bit resolution adc leads to 4932 counts per revolution, or resolution of  $0.073^\circ$ . The joint angle estimate resolution is, assuming no slip of the drive<sup>3</sup>, the resolution of the rotor position divided by the gear ratio, which is taken in this case to be approximately 20:1. Therefore the effective joint angle estimate resolution is  $9e-3^\circ$  resulting in a worst case endpoint resolution of 0.9mm, which is quite sufficient for sensorimotor tasks such as manipulation and locomotion.

Brushless DC motors require precise absolute position feedback in order to be properly electronically commutated. In order to minimize torque ripple introduced by the method of block commutation, sinusoidal commutation is used to smoothly commutate the motors. Torque ripple is highly

<sup>3</sup>Cable drives are often used in haptic and bio-mimetic robotic applications, but sometimes suffer from slippage.

undesirable in a system to be used for manipulation and locomotion.

### III. COMBINING HALL EFFECT SENSOR POSITION ESTIMATES WITH BLOCK, SINUSOIDAL, AND ADAPTIVE SINUSOIDAL COMMUTATION METHODS.

#### A. Block commutation

The simplest method of commutating a BLDC motor is 'trapezoidal' or 'block' commutation. This in general consists of a few steps, beginning with measuring rotor position via (high or low resolution) Hall sensors, optical or magnetic encoders, or back-EMF (bEMF) generated by each coil. When low resolution Hall sensors are used in common applications, a rotor-position-dependent code (Fig. 5) is present in the Hall sensor data (typically Hall sensor outputs are filtered to be a binary signal - here referred to as digital Hall sensor circuits or DHS). In stages, a pair of coils are connected in such a way as to allow current to flow between the two coils, forming a field which draws the rotor to rotate to align opposing fields. As the rotor rotates, the Hall sensor 'code' changes, and the current is altered to flow through appropriate pairs of coils to continuously draw the rotor toward the moving field. It is important to note that this switching of the field flow leads to a torque ripple effect which is dependent on several motor parameters (most notable are rotor position and speed) in terms of peak-to-peak wave amplitude. This method of commutating BLDC

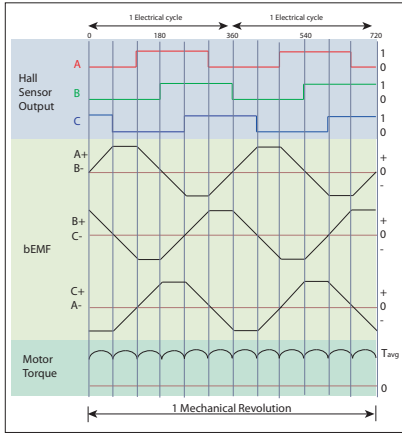


Fig. 5. This denotes block commutation over one mechanical revolution for a typical three-phase BLDC motor with trapezoidal bEMF (adapted from AN885 technical note document from microchip.com). The torque ripple due to commutation is evident, and is undesirable for fine bio-mimetic control experiments.

motors is therefore more desirable in situations in which motor speed will tend to be higher and more constant because the torque ripple is velocity dependent due to the inertia and the time constant of the motor. In the case dealing with locomotion and object manipulation using highly sensitive robotic systems, RPMs tend to be low or nearly zero, directions change frequently, and the motor occasionally will be stalled. A commutation method which creates a smooth transition between stator pole locations must be employed.

Sinusoidal commutation is appropriate for low speeds, and in many bio-mimetic[7][11] robotic applications (manipulation and locomotion), speeds are relatively low, though torques may be high.

#### B. Method of sinusoidal commutation

The maximum torque upon the rotor can be exerted when one of the poles is positioned directly between a pair of coils

which are creating a field of opposing magnetic orientation. Considering the coordinate system of the rotor, the force due to the field generated in the coil acting upon the rotor can be decomposed into a tangential component and an orthogonal component which creates a torque balanced by the motor bearings as opposed to causing a rotation.

If the fields of the coil and permanent magnets are aligned, the rotor will be stationary. If they are misaligned slightly, a torque will act to rotate the rotor until they are aligned. If the misalignment is perpetuated by rotating the coil-based field ahead of the rotor's rotation, a continuous, cog-free rotation of the rotor occurs. The torque generated will be determined by the amplitude of the sinusoids (which, in a digital system, can be realized via PWM), as well as the degree of phase shift of the active fields.

The fields are a sinusoidal function of rotor angular position, with each coil phase-shifted (since each coil in a three-phase motor is physically phase shifted by 60 or 120 degrees) and then phase shifted relative to rotor position. This rotor position phase shift can be constant or dynamic - a function of rotor speed. The relations are given (where A, B, and C are the coil PWM commands for coil A, B, and C respectively,  $\hat{\theta}$  is the rotor angle estimate,  $\phi$  is the 'shift' of all sensors relative to a midpoint between coils,  $\psi_i$  is the placement of the second and third sensors relative to the first, M is the command, and  $\rho$  is the phase advance desired by the engineer tuning the system) by

$$\begin{aligned} A &= M \sin(\hat{\theta} - \phi + \rho), \\ B &= M \sin(\hat{\theta} - \phi + \rho - \hat{\psi}_1), \\ C &= M_{max} - A - B. \end{aligned} \quad (8)$$

Note that, since total current entering and leaving the system must be zero, C is a driven quantity.

To rotate in the opposing direction, one must merely compute the complement of the first two equations (the third is still driven):

$$\begin{aligned} A &= M_{max} - M \sin(\hat{\theta} - \phi + \rho), \\ B &= M_{max} - M \sin(\hat{\theta} - \phi + \rho - \hat{\psi}_1), \\ C &= M_{max} - A - B. \end{aligned} \quad (9)$$

#### C. Parameter estimation via Extended Kalman Filter

Several parameters associated with controlling the motor for maximum torque generation include individual Hall sensor position, phase shift, maximum and minimum for each sensor. Since the main parameters have simple state-dependent nonlinear dynamics, they can be estimated by an EKF with 'fast' noise processes driving them to a zero estimation error. It is emphasized again here that the EKF is not necessarily needed if one is most concerned about a simple application, but it is presented for added precision and to improve performance. In many cases, simply computing an angle based on what was discussed earlier and directly using that for commutation is effective. The EKF makes the general methodology applicable in more cases than otherwise possible. We need to estimate  $\phi_i$ ,  $\alpha_i$ , and  $\beta_i$  for all i, knowing only the ideal and initial conditions. We also want to use these estimates to estimate  $\theta$  as well.  $\alpha_i^0$  and  $\beta_i^0$  are computed after power-up during an initialization routine. Then all the parameters must be gradually adjusted over time (e.g. the Hall sensors may shift with temperature which affects magnitude and phase). The future estimates are propagated by a discrete EKF[3][1][10] with continuous dynamics and observation model. Noise processes are assumed to be Gaussian, with mean 0 and covariance  $\Omega$ .

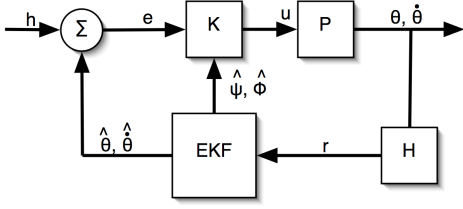


Fig. 6. Block diagram depicting estimated, measured, and computed quantities in the adaptive control scheme. The control, K, can include block, sinusoidal, or field oriented control. Here  $h$  represents the reference,  $e$  the error signal, P the plant, items with hats are estimated,  $\theta$  and  $\dot{\theta}$  are position and velocity, respectively,  $\phi$  and  $\psi$  represent Hall sensor placements and phase angles, respectively, H the Hall sensors, and  $r$  the Hall sensor signals.

In order to control the BLDC motor in the face of uncertainties we need to include the following states:

- $q$  - The number of  $\pi/2$  quadrants traversed since the last reset of the estimator.
- $\hat{\theta}$  - The rotor angle estimate in mechanical revolution space.
- $\hat{\dot{\theta}}$  - The rotor angular velocity estimate in mechanical revolution space.
- $\hat{\phi}$  - The mean of the estimate of all of the Hall sensor phase angles.
- $\hat{\psi}_i$  - The mean of the estimate of the individual Hall sensor placements relative to the others.
- $\sigma_\phi$  - The covariance of the estimate of phase angles.
- $\sigma_{\psi_i}$  - The covariance of the estimate of the individual phase angles of the sensors relative to each other.
- $\tau$  - Motor command state (can be implemented as position, velocity, or torque depending on requirements).
- $\alpha_i$  - The minimum Hall sensor measurement for sensor  $i$ .
- $\beta_i$  - The maximum Hall sensor measurement for sensor  $i$ .
- $r$  - The normalized Hall sensor measurement values.
- $\bar{r}$  - The raw Hall sensor measurement values
- $\zeta$  - The motor reference (can be implemented as position, velocity, or torque depending on requirements).

The state dynamics are augmented with the Kalman filter dynamics as in [9]. The state is then:

$$x = [q, \hat{\theta}, \hat{\dot{\theta}}, \sigma_\theta, \sigma_{\dot{\theta}}, \hat{\phi}, \hat{\psi}_i, \sigma_\phi, \sigma_{\psi_i}, \tau, \alpha_i, \beta_i, r, \zeta]^T \quad (10)$$

The state estimate propagation and error covariance propagation are combined into one matrix, using the relations defined in the above Sections, to form

$$\dot{\hat{x}}(t) = \begin{bmatrix} \left[ \frac{1.8|\hat{\dot{\theta}}|}{\pi} \right] \text{sign}(\hat{\dot{\theta}}) \\ \hat{\dot{\theta}} \\ -J^{-1}(k_e + \mu_f)\hat{\dot{\theta}} \\ 2\hat{\dot{\theta}}\sigma_\theta + \Omega_\theta \\ -2J^{-1}(k_e + \mu_f)\hat{\dot{\theta}}\sigma_{\dot{\theta}} + \Omega_{\dot{\theta}} \\ 0 \\ 0 \\ \Omega_\phi \\ \Omega_{\psi_i} \\ 0 \\ 0 \\ 0 \\ 0 \\ 0 \\ 0 \end{bmatrix}, \quad (11)$$

with the definitions  $k_e$  (Motor back EMF constant -  $Nm/\hat{\theta}$ ),  $J$  (Rotor inertia -  $kg \cdot m^2$ ), and  $\Omega$  (noise covariance with a subscript denoting the state to which each one refers - ie  $\Omega_\phi$  is the noise covariance for the estimate of  $\phi$ ).

The Kalman gains are computed (at timestep  $k$  before the sample update  $'(-)'$  but omitted for notational clarity) as follows, with  $\Delta$  defined as a temporary symbol below,

$$\begin{aligned} K_{\theta_k} &= n\sigma_{\theta_k}\hat{\dot{\theta}}_k \cos(n(\hat{\theta}_k - \hat{\phi}_k)), \\ &* [n^2\sigma_{\theta_k}\hat{\dot{\theta}}_k^2 \cos^2(n(\hat{\theta}_k - \hat{\phi}_k)) + \Omega_{y_\theta}]^{-1}, \\ \Delta &= n[\hat{\dot{\theta}}_k \cos(n(\hat{\theta}_k - \hat{\phi}_k)), \\ &- \hat{\dot{\theta}}_{k-1} \cos(n(\hat{\theta}_{k-1} - \hat{\phi}_{k-1}))], \\ K_{\dot{\theta}_k} &= \sigma_{\dot{\theta}_k} \Delta (\sigma_{\dot{\theta}_k} \Delta^2 + \Omega_{y_\theta})^{-1}, \\ K_{\sigma_{\theta_k}} &= K_{\theta_k}, \\ K_{\sigma_{\dot{\theta}_k}} &= K_{\dot{\theta}_k}, \\ K_{\phi_k} &= -n\sigma_{\phi_k} \cos(n(\hat{\theta}_k - \hat{\phi}_k)), \\ &* (n^2\sigma_{\phi_k} \cos^2(n(\hat{\theta}_k - \hat{\phi}_k)) + \Omega_\phi)^{-1}, \\ K_{\psi_{i_k}} &= -n\sigma_{\psi_{i_k}} \cos(n(\hat{\theta}_k - \hat{\phi}_k - \hat{\psi}_{i_k})), \\ &* (n^2\sigma_{\psi_{i_k}} \cos^2(n(\hat{\theta}_k - \hat{\phi}_k - \hat{\psi}_{i_k})) + \Omega_{\psi_{i_k}})^{-1} \\ K_{\sigma_{\phi_k}} &= K_{\phi_k}, \\ K_{\sigma_{\psi_{i_k}}} &= K_{\psi_{i_k}}. \end{aligned} \quad (12)$$

Now we define a composite Kalman gain,  $K \in \mathfrak{R}^{n_x \times n_x}$ , which will be a diagonal matrix,

$$K_k = \text{diag}\{0, K_{\theta_k}, K_{\dot{\theta}_k}, 0, K_{\sigma_{\theta_k}}, K_{\sigma_{\dot{\theta}_k}}, K_{\phi_k}, K_{\psi_{i_k}}, 0, K_{\sigma_{\phi_k}}, K_{\sigma_{\psi_{i_k}}}, 0\}. \quad (13)$$

We define, for space considerations, the vector  $d\omega \in \mathfrak{R}^{n_x \times 1}$  to represent the errors between observation and predictions (for the portions related to state measurement update), and the error covariance update magnitude (for the portions related to error covariance update), where all variables are pre-update (except for the  $k-1$  variables), but the  $'(-)'$  is omitted for notational clarity,

$$\begin{aligned} d\omega_\theta &= r_0 - \sin(n(\hat{\theta}_k - \hat{\phi}_k)), \\ d\omega_{\dot{\theta}} &= (r_k - r_{k-1}) - (\sin(n(\hat{\theta}_k - \hat{\phi}_k)), \\ &- \sin(n(\hat{\theta}_{k-1} - \hat{\phi}_{k-1}))), \\ d\omega_{\sigma_{\theta_k}} &= -n\sigma_{\theta_k}\hat{\dot{\theta}}_k \cos(n(\hat{\theta}_k - \hat{\phi}_k)), \\ d\omega_{\sigma_{\dot{\theta}_k}} &= -n\sigma_{\theta_k}[\hat{\dot{\theta}}_k \cos(n(\hat{\theta}_k - \hat{\phi}_k)), \\ &- \hat{\dot{\theta}}_{k-1} \cos(n(\hat{\theta}_{k-1} - \hat{\phi}_{k-1}))], \\ d\omega_{\phi_k} &= r_0 - \sin(n(\hat{\theta}_k - \hat{\phi}_k)), \\ d\omega_{\psi_{i_k}} &= (r_0 - r_1), \\ &- (\sin(n(\hat{\theta}_k - \hat{\phi}_k)) - \sin(n(\hat{\theta}_k - \hat{\phi}_k - \hat{\psi}_{i_k}))), \\ d\omega_{\sigma_{\phi_k}} &= n\sigma_{\phi_k} \cos(n(\hat{\theta}_k - \hat{\phi}_k)), \\ d\omega_{\sigma_{\psi_{i_k}}} &= n\sigma_{\psi_{i_k}} \cos(n(\hat{\theta}_k - \hat{\phi}_k - \hat{\psi}_{i_k})). \end{aligned} \quad (14)$$

The state estimate update and error covariance update are combined into one set of calculations in the following way,

$$\begin{bmatrix} 0 \\ \hat{\theta}_k(+), \hat{\dot{\theta}}_k(+), \sigma_{\theta_k}(+), \sigma_{\dot{\theta}_k}(+), \hat{\phi}_k(+), \hat{\psi}_{i_k}(+), \sigma_{\phi_k}(+), \sigma_{\psi_{i_k}}(+), 0 \end{bmatrix} = \begin{bmatrix} 0 \\ \hat{\theta}_k(-), \hat{\dot{\theta}}_k(-), \sigma_{\theta_k}(-), \sigma_{\dot{\theta}_k}(-), \hat{\phi}_k(-), \hat{\psi}_{i_k}(-), \sigma_{\phi_k}(-), \sigma_{\psi_{i_k}}(-), 0 \end{bmatrix} + K_k \begin{bmatrix} 0 \\ d\omega_{\theta_k}, d\omega_{\dot{\theta}_k}, d\omega_{\sigma_{\theta_k}}, d\omega_{\sigma_{\dot{\theta}_k}}, d\omega_{\phi_k}, d\omega_{\psi_{i_k}}, d\omega_{\sigma_{\phi_k}}, d\omega_{\sigma_{\psi_{i_k}}}, 0 \end{bmatrix}. \quad (15)$$

The variable phase  $\phi$  can be omitted from this part of the estimation and held constant, tuned during a startup procedure, or allowed to drift only slowly, as it is mainly a torque maximizing variable. Thus if all the other parameters converge to the correct value, and  $\phi$  is slightly non-optimized, the motor will function. It merely will not function at peak torque capability. If the value moves outside of about  $\pi/2$  Radians, the torque generated in the BLDC motor will swap sign, and excessive current flow and coil temperature increases will occur.

Now that the estimation scheme has been developed, and since it is separate from the commutation scheme employed, the estimates coming out of the EKF can be used with any commutation scheme. In Fig. 6, the commutation scheme is lumped within the control  $\mathbf{K}$ .

#### D. Other issues to consider

After all this work developing a commutation method for precision control and minimization of ripple, it would be disconcerting to implement the system and have other factors cause ripple and imprecision. We will now consider two other issues - a simple way to deal with friction and other nonlinearities, and how to choose PWM cycle frequency.

1) *Reducing ripple due to friction and nonlinearities in the electronics by local feedback:* Since friction and electronics such as the intrinsic freewheeling diodes contribute nonlinear effects to the motor dynamics, a local proportional feedback controller is implemented to account for these effects - taking in a particular current command, and outputting a PWM command. The actual coil current is measured with the use of high precision current sensing resistors. This measure is used as a feedback signal to drive the system to desired levels and prevent excess current flow (Fig. 7).

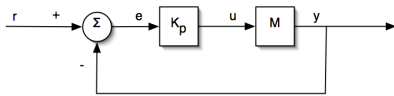


Fig. 7. Local feedback control helps cancel nonlinearities due to friction, and nonlinear electrical characteristics in the motor.

The controller can be a P, PI, PD, or PID controller. Even if a proportional control is used, performance can improve significantly. The gain is set using a standard classical control method - find the gain at which the system becomes unstable and then reduce the gain by an arbitrary factor such as one half. A good treatment of related nonlinear phenomena is given in [2], and an example of improvement with an interesting application is given in [4].

#### E. Choosing PWM cycle frequency to minimize ripple

The cycle frequency for the PWM is computed by considering characteristics of the physics of the motor used.

PWM is based on the fact that the motor, due to its inertia and LR (Inductance and resistance) characteristics, acts as a low pass filter. A repeating square wave input current of varying frequencies will be filtered to a DC current between the maximum voltage and zero volts. The period of one of the PWM wave cycles determines the smoothness of the DC average current, as a function also of motor characteristics (inductance and resistance).

The less smooth the current waveform in the motor, the greater the power loss. Control performance and smoothness of movement at low speeds are negatively affected as well. Let us consider energy loss as an indirect measure of smoothness here. Energy is lost during the switching time of the transistors, the resistance in the windings of the motor, and wires in the system.

To quantify the losses due to lack of smoothness of the current waveform we perform a simple example. If the current of a perfect DC signal in the motor is  $I$ , the power dissipation due to the motor, component, and wire resistances is given by

$$P = I^2 R \quad (16)$$

However a 50:50 square wave (we assume a perfect square wave of current moving through the motor for simplicity of calculations) with a maximum current of  $2I$  and minimum of zero would produce the relation

$$P = (2I)^2 R/2 + (0)^2/2 = 2I^2 R \quad (17)$$

This is double the energy loss. Thus it is desirable to achieve as smooth a DC current waveform in the motor as possible for efficiency<sup>4</sup> and low ripple.

The required switching frequency can be computed as a function of motor parameters in order to achieve a desired percent of fluctuation of the current waveform. It can easily be shown from the equation derived from an LR circuit that this relationship is given by

$$f = \frac{-R}{2L \cdot \ln(1 - P/100)} \quad (18)$$

or, defining ripple percent  $A_r = (1 - P/100)$ . This requires knowing or measuring motor parameters of inductance ( $L$ ) and resistance ( $R$ ). The inductance and resistance of the example BLDC motor is given to be  $0.36mH$  and  $3.75\Omega$ . A ripple percentage (for a constant desired average current) vs. PWM frequency plot becomes an inverse logarithmic relation shown in Fig. (8). Thus for this motor, a ripple amplitude of

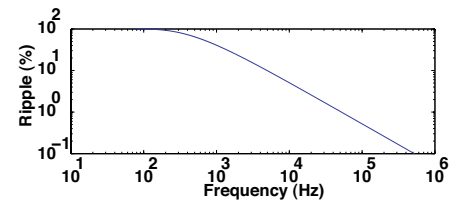


Fig. 8. Power dissipation percent vs. PWM cycle frequency for  $R=3.75\Omega$  and  $L=0.36mH$ . Required PWM frequency can be determined by this plot and the required power dissipation.

1% would be possible with a PWM frequency of 51.8kHz.

<sup>4</sup>Power for mobile robotics is often onboard, so energy waste should be minimized

Since the power amplification circuitry employed has an absolute maximum PWM frequency of 50kHz, the minimum ripple amplitude possible at this rate is 3.5%, which is still acceptable. It should be noted that increasing PWM frequency reduces effective resolution of the PWM duty cycle. The relation [6] is given by (with  $\gamma$  defined as resolution)

$$\gamma = \frac{\log(2T_{PWM}/T_{CY})}{\log(2)}. \quad (19)$$

Here 'resolution' is in bits. Thus the effective PWM resolution at a frequency of 10kHz is roughly 4000, while at 40kHz reduces to 1000. The PWM frequency can be adjusted by altering one or both parameters of the motor included in this equation - namely the resistance and inductance. We achieve satisfactory performance with this PWM frequency.

#### IV. RESULTS

##### A. Hall sensor-based measurements

The position measurements from the Hall sensors (such as Fig. 9(c)) are compared to measurements from a 12-bit quadrature encoder which are coupled to the motor with a position test setup. The sampling was performed at 1kHz, and the data was communicated to the host computer at 200Hz (due to the multiple 16-bit variables). The frequencies of interest lie in the Hz range, so sampling roughly 100 times faster provides a good measure here. It is clear that the two measures are comparable, with a mean absolute error of 0.073 Rad (Fig. 9(a) and 9(b)).

##### B. Coil field interference with Hall sensor vs. orientation to field

In this experiment, random noise was injected into a coil. A Hall sensor was mounted at variable positions from orthogonal to the wide axis of the coil (orthogonal to the field) to in line with the field generated by the coil. Then data points were recorded of the angle and average voltage from the Hall sensor. Fig. 9(d) shows that the Hall measurements are dominated by the rotor field. No matter what orientation the Hall sensor is placed at, the amount of magnetic flux density measured due to the field in the coils is minimal. It is postulated that this can be attributed to the magnetic circuit - essentially very little magnetic flux from the coils is escaping the motor's lower reluctance materials. However, the magnetic field created by the rare earth magnets in the rotor does escape the motor's materials and thus is quite easy to measure.

The experimental apparatus allowed for slight variation in the position of the Hall sensor, which affected the outcome of each trial. The data displayed represents approximately fifteen trials to remove individual effects as much as possible, but the moving average used to smooth the data is influenced by outliers.

##### C. Comparison of control approaches using Hall sensor-based measurements

The BLDC motor was controlled with block, and sinusoidal commutation and the results are compared in Fig. 10.

The analog measurements from this sensor arrangement provide a good high resolution position measurement, demonstrating that this methodology can essentially be applied to any desired commutation scheme.

In Fig. 10, we see that block commutation, in general, has higher ripple amplitudes than sinusoidal commutation, as expected. The mounting method for the sensors may have some phase shift in terms of angle relative to the coils, so the sinusoidal commutation still has some residual ripple from

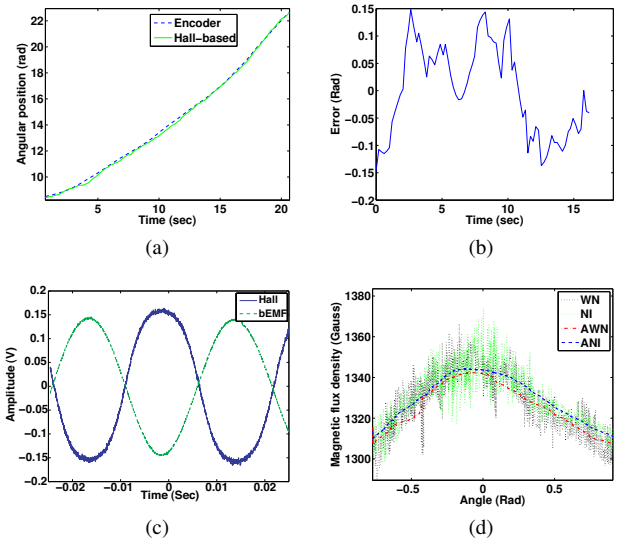


Fig. 9. (a) Hall sensor-based position estimates versus a quadrature encoder. The two signals are quite close, with an average absolute error of 0.073 Rad (average error is 0.029 Rad). Data is sampled at 500Hz and rotor is manually rotated by a human experimenter. (b) Error in radians between the two measurement methods. The Hall sensor estimates may actually be closer to the correct value than the encoder since the encoder's interface was a software one. It is possible counts were missed in the encoder measurements. (c) Hall sensor signal scaled to comparable levels with a single coil's bEMF during a constant angular velocity. Note that the Hall signal is inverted relative to the bEMF, but in phase. Also note that both the Hall signal and bEMF are sinusoidal. (d) Plot legend entries refer to: WN - White noise, NI - No input, AWN - Averaged white noise (data is averaged to smooth), ANI - Averaged no input. Magnetic flux densities as measured by the precision linear Hall sensor (same model used to commutate the motor). One data set is due to varying the angle of the Hall sensor while the current command sent to all three coils is white noise. The second data set is provided by performing the same experiment with no coil currents, only the rotor field is present in this case. Clearly the effects of the coil magnetic field are minimal - the rotor field dominates.

commutating slightly off-phase in the coils. This is where the estimator would account for these variations, and future work will implement the estimator in realtime.

##### D. EKF-based adaptive position estimation

The performance of the estimation in simulation is shown in Fig. 11 for multiple initialization of all parameters. Since the parameters should drift slowly, a period of time is required initially for convergence, after which the values change little. However, this time can be quite short - here it takes less than 400 msec before convergence, with conservative drift rate parameters. Current estimates can be saved for the next power-up of the motor driver in order to facilitate more rapid initialization.

The estimator is capable of determining unknown placement parameters, maximum and minimum Hall sensor values, angular position, and angular velocity. The values of the parameters converge in approximately two seconds. As with all EKF-based estimators, convergence rate is determined by filter parameters such as the covariance of the noise, however the approximate nature of the EKF can be sensitive to filter parameter adjustments in a stability sense.

As can be seen in Fig. 11(a)-11(d), from any one Hall sensor, all three measures can be reconstructed using the mean of the EKF parameter estimates effectively.

It would be possible to also integrate the bEMF into the EKF, as this is additional information, when the motor is moving at a high enough velocity. The advantage would be that this measure is always correctly in phase, as opposed to

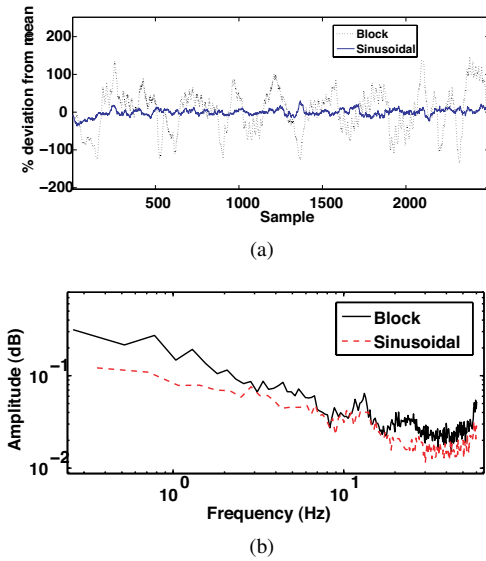


Fig. 10. (a) Block and sinusoidal commutation (no adaptive estimation) at constant velocity command (no feedback). The DC constant is removed, and the values shown are in % deviation from the average velocity. The sensor mounting is assumed to be perfectly symmetrical and properly centered. Note that sinusoidal commutation produces a much lower ripple than block commutation. (b) Block and sinusoidal commutation scheme rotor angular velocity frequency components with DC components of signal removed. The remainder of the signal, if commutation were smooth, should fall off like a first order system. It is clear that the sinusoidal commutation scheme has less resonance peaks than the block commutation scheme, as expected.

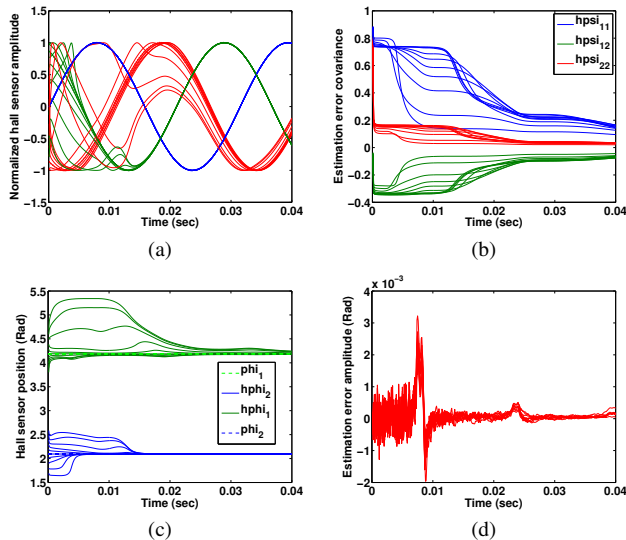


Fig. 11. (a) Shows the actual vs. estimated Hall sensor measurements. The estimates quickly converge to the correct value and track well during this constant velocity test. (b) Shows the convergence of the error covariance values. (c) Shows the convergence of the mean estimates for  $\phi$ . (d) Shows the Estimation error amplitude for the position of the BLDC motor's rotor.

the Hall sensors which may be poorly mounted or damaged. However, one would need to take into account the bEMF profile (trapezoidal or sinusoidal) for contributing to the position estimate when building the mathematical model. The disadvantage is added complexity of programming, the fact that the algorithm would need to be tailored to each motor, and computational complexity would increase, which is the reason this has not been integrated here. Future experiments will include bEMF measures to determine the impact regarding the issues just mentioned. It is also worth briefly stating that the EKF runs the sensor parameter estimation portion at a much lower rate than the position estimation, since to commutate the motor at any significant velocity requires rapid updates, and the sensor parameters change little, so one could save computation time and only update the sensor parameters every so often.

## V. CONCLUSION

We have developed a novel method of measuring position for brushless motor applications which is useful in highly compact spaces with small motors such as pancake motors. This method uses high precision (but low cost) linear Hall sensors to effectively measure rotor magnetic flux while, as we showed, rejecting interference by the coil fields. It was demonstrated that this method of measurement can be implemented on an inexpensive embedded processor (the dsPIC33FJ256MC710 in this case, but many varieties are possible) in realtime while the processor performs other tasks as well. Furthermore, the estimation method proposed can improve measurement accuracy and commutation smoothness. This allows for inexpensive mounting of the Hall sensors in such a way that position parameters vary, and the possibility of compensating for other parameters which may drift over time. What this means overall is that an integrated actuator can be produced which has minimal cost, high accuracy, and can be deployed in highly compact applications.

## REFERENCES

- [1] B. Anderson and J. Moore. *Optimal Filtering*. Prentice Hall, 1979.
- [2] J. Fiene and G. Niemeyer. Switching motor control: An integrated amplifier design for improved velocity estimation and feedback. *In proc. IEEE Int. Conference on Robotics and Automation*, 5:4504–4509, April 2004.
- [3] A. Gelb, editor. *Applied Optimal Estimation*. The MIT Press, 1984.
- [4] G. Graham. Practical design and stabilizing control of a dynamic balancing and flipping robot. Master's thesis, University of California, San Diego, La Jolla, CA, 2007.
- [5] T. Massie. Design of a three degree of freedom force-reflecting haptic interface. Master's thesis, Massachusetts Institute of Technology, Cambridge, MA, 1996.
- [6] Microchip. *dsPIC33FJXXXMCX06/X08/X10 Motor Control Family Data Sheet*. Microchip, inc., 2007.
- [7] D. Paluska, M. Mataric, and R. Ambrose. *Biologically Inspired Intelligent Robots*, volume PM122, chapter Biomimetic Robot Control. SPIE Press, May 2003.
- [8] A. Simpkins. *Exploratory studies of human sensorimotor learning with system identification and stochastic optimal control*. PhD thesis, University of California at San Diego, La Jolla, CA, 2009.
- [9] A. Simpkins, R. A. de Callafon, and E. Todorov. Optimal tradeoff between exploration and exploitation. *In Proc. of the American Control Conference, 2008*, pages 33–38. IEEE Computer Society, June 2008.
- [10] H. W. Sorenson, editor. *Kalman Filtering: Theory and Application*. IEEE Press, 1985.
- [11] E. Todorov and M. Jordan. Optimal feedback control as a theory of motor coordination. *Nature Neuroscience*, 5(11):1226–1235, 2002.
- [12] J. M. Vandeweghe, M. Rogers, M. Weissert, and Y. Matsuoka. The act hand: Design of the skeletal structure. *Proc. 2004 IEEE Int. Conference on Robotics and Automation (ICRA '04)*, May 2004.
- [13] D. Wilkinson, J. M. Vandeweghe, and Y. Matsuoka. An extensor mechanism for an anatomical robotic hand. *Proc. 2003 IEEE Int. Conference on Robotics and Automation (ICRA '03)*, 1:238 – 243, May 2003.
- [14] P. Yedamale. An885: Brushless dc (blbc) motor fundamentals. Application note, Microchip Technology inc., 2003.
- [15] J. Zambada. An1078: Sensorless field oriented control of pmsm motors. Application note, Microchip Technology inc., 2007.